TTF1-NPs Induce ERS-Mediated Apoptosis and Inhibit Human Hepatoma Cell Growth In Vitro and In Vivo

Bin Xiao,*[1] Chao Liu,*†[1] Bing-tong Liu,*[1] Xuan Zhang,* Rong-rong Liu,* and Xue-Wu Zhang*

*College of Medicine, Yanbian University, Yanji, Jilin Province, China
†Affiliated Hospital, Yanbian University, Yanji, Jilin Province, China

Previous studies have shown that 5,2′,4′-trihydroxy-6,7,5′-trimethoxyflavone (TTF1) is the primary anticancer constituent of the traditional Chinese medicinal plant *Sorbaria sorbifolia* (SS), which has been applied to treat cancer in China. In this study, we investigated the in vitro and in vivo antitumor effects and biological mechanisms of small-molecule TTF1 nanoparticles (TTF1-NPs). The effects of TTF1-NPs on cell growth and apoptosis were investigated using human hepatoma cells. The molecular changes associated with the effects of TTF1-NPs were analyzed by immunocytochemistry and Western blot analysis. The in vivo effect of TTF1-NPs was investigated using the HepG2 tumor xenograft model. We found that TTF1-NPs exhibited antitumor effects in vitro accompanied by induction of apoptosis in human hepatoma cells. Mechanistically, our data showed that TTF1-NPs induced apoptosis via endoplasmic reticulum stress (ERS) pathway in hepatoma cells. Moreover, inhibition of ERS activation blocked TTF1-NP-induced apoptosis in HepG2 cells. Finally, TTF1-NPs inhibited the growth of HepG2 xenograft tumors. Taken together, our results demonstrated that TTF1-NP-induced apoptosis was mediated at least in part by the ERS pathway and thus inhibited hepatoma tumor growth.

Key words: *Sorbaria sorbifolia*; Traditional chinese medicine; Hepatoma; TTF1;
Endoplasmic reticulum stress; Apoptosis; HepG2; Nanoparticles

INTRODUCTION

Liver cancer is the third leading cause of cancer-related mortality and the sixth most common type of neoplasm. The most common form of liver cancer in adults is hepatocellular carcinoma (HCC, also known as malignant hepatoma), which causes more than 600,000 deaths annually, about half of which are in China (1). The incidence of HCC as a primary liver cancer is closely associated with the incidence of hepatitis (2), and this cause is more common in Asia and Africa. In contrast, most liver cancers in patients in North America and Western Europe are metastases from tumors elsewhere in the body. Although the etiology of HCC varies widely according to geographic location, it has an extremely poor prognosis, and death usually occurs within a period of 3–6 months (3,4).

The poor prognosis associated with HCC is partially due to the limited treatment options available to clinicians. Only 30–40% of HCC patients are considered eligible for treatment, which may include chemoembolization, surgical resection, or liver transplantation, and only 10–20% of HCCs may be entirely removed by surgery. Although most HCC patients will receive chemotherapy at some point during treatment as a means of prolonging life, most currently used drugs show limited efficacy (5,6). Doxorubicin was used for many years as the primary chemotherapeutic agent for HCC patients despite a response rate of only 15–20%, and other agents, including epirubicin, cisplatin, and fluorouracil, show even lower efficacy (6). Sorafenib, the first agent approved by the US FDA for the treatment of advanced HCC, improved median survival and time to progression by 3 months, but showed no effect on quality of life measures, possibly due to its toxicity (7).

The toxicity and limited efficacy of current treatments for patients with HCC has led to significant research efforts focused on developing drugs with fewer side effects and greater therapeutic efficacy. Much of this effort has been dedicated to exploring the anticancer potential of compounds isolated from natural products (8). Natural products have been used in Western medicine to treat cancer for more than 40 years, and more than 60% of the clinically used antitumor compounds approved since 1940 are

---

natural products or are derived from them. In the search for new drugs from natural sources, traditional Chinese medicine has proven to be an excellent source from which lead compounds can be identified due to millennia of documented use of a diverse array of natural products.

The medicinal plant *Sorbaria sorbifolia* (SS), commonly known as False Spiraea, has been traditionally used as an anticancer therapy in the area surrounding Changbai Mountain in China. In previous studies, acetic ether extracts of SS inhibited the growth of HepG2 and mouse 180 sarcoma cells and downregulated p53 and Bcl-2. Recently, we found that 5,2′,4′-trihydroxy-6,7,5′-trimethoxyflavone (TTF1) is the major anticancer bioactive constituent of SS, and we showed that TTF1 inhibited angiogenesis in chick embryo chorioallantoic membranes and induced apoptosis in HepG2 cells via a mitochondrial pathway (9,10). However, in vivo evaluation of TTF1 as a potential anticancer drug has been limited by its low absorbance and high biodegradability.

To address these limitations of TTF1, we prepared biodegradable small molecule TTF1 nanoparticles (TTF1-NPs) using an emulsion evaporation–solidification method at low temperature, allowing us to study the in vivo anti-hepatoma effects of TTF1 and its underlying molecular mechanism. In this study, we evaluated the effects of TTF1-NPs on hepatoma cells and in a nude mouse HepG2 xenograft model. In addition, because we showed in a previous report that TTF1 induced apoptosis in HepG2 cells via a mitochondrial pathway, we also explored ERS-meditated apoptosis as a potential antihepatoma mechanism for TTF1-NPs.

MATERIALS AND METHODS

Preparation of TTF1-NPs

TTF1 was isolated from 10 kg of SS (collected from Yanji, Jilin Province, China) using water extraction and alcohol (WAE) precipitation as previously reported (9). Biodegradable, small-molecule (average particle diameter, 195.2 ± 35.2 nm; average entrapment efficiency, $64.57 \pm 8.21\%$) TTF1-NPs were prepared with a stearic acid solid lipid nanostructured carrier using an emulsion evaporation–solidification method at low temperature, as previously reported. The TTF1-NPs were highly soluble, and TTFI diffusion was characterized by an initial stage of burst release (11,12).

Cell Culture and TTF1-NP Treatment

Human hepatoma cell lines (HepG2, Hep3B, and PLC/PRF/5) were purchased from KeyGEN Co., Ltd. (Nanjing, China) and cultured in Dulbecco's modified Eagle's medium (DMEM; Gibco, Shanghai, China) supplemented with 10% fetal bovine serum (FBS; Gibco, Shanghai, China), 100 U/ml penicillin, and 100 mg/L streptomycin at 37°C in a humidified incubator with a 5%

CO_2 atmosphere. Cells in the logarithmic growth phase were transferred to 96-well plates (6×10^3/well). After 24 h of growth, adherent cells were treated as follows: 50, 100, or 200 μM TTF1-NPs for the TTF1-NP treatment groups; 10 μM 5-fluorouracil (5-FU) for the positive control group; and DMEM medium for the negative control group (vehicle). The cells were assayed after 24, 48, and 72 h of exposure to the appropriate treatment. For the assays of HepG2 cells using the ERS inhibitor 4-phenylbutyrate (4-PBA), 5 mM 4-PBA was added to cells treated with 200 μM TTF1-NPs or DMEM medium after 24 h, and the cells were cultured for a further 48 h.

MTT Assay

The effect of TTF1-NP treatment on cell growth was assessed in three human hepatoma cell lines (HepG2, Hep3B, PLC/PRF/5, and human liver cells) using the MTT assay. The cells were treated with TTF1-NPs (50, 100, or 200 μM), 5-FU (positive control), or vehicle after 24 h, and the MTT assay was performed after 48 and 72 h. Briefly, the cells were exposed to MTT (0.5 mg/ml) for 4 h at 37°C, 180 μl of DMSO was added, and the optical density (OD) was measured at 490 nm with a spectrophotometer (Thermo Fisher, Shanghai, China). The cell growth inhibition ratio (%) was calculated as follows:

$$\text{cell growth inhibition ratio } (\%) = (\text{OD}_{vehicle} - \text{OD}_{treatment}) / \text{OD}_{vehicle} \times 100$$

where $\text{OD}_{vehicle}$ is the OD of the vehicle group and $\text{OD}_{treatment}$ is the OD of the treatment group.

Cell Morphology Observation

HepG2 cells were treated with TTF1-NPs (50, 100, or 200 μM), 5-FU (positive control), or DMEM (vehicle) for 48 h, and staining was performed with hematoxylin and eosin (H&E) and Hoechst 33258 stain. Briefly, the cells were fixed for 20 min using 4% paraformaldehyde, washed with PBS, and stained. For H&E staining, the cells were exposed to hematoxylin for 3 min and eosin for 1 min, washed with water, dehydrated with an alcohol gradient, exposed to xylene for 15 min, dried, and mounted on slides with neutral balsam for microscopic observation. For Hoechst 33258 staining (KeyGEN Co., Ltd., Nanjing, China), the cells were stained for 10 min, washed with PBS, dried in the dark, and observed using a fluorescence microscope.

Flow Cytometry Assay

To measure apoptosis, HepG2 cells treated with TTF1-NPs (50, 100, or 200 μM; with or without 4-PBA), 5-FU (positive control), or vehicle (with or without 4-PBA) for 48 h were analyzed by flow cytometry. Briefly, the cells (1×10^6 per well) were stained [10 μl annexin V and 5 μl propidium iodide (PI)] and analyzed using a flow cytometer (Becton Dickinson, Franklin Lakes, NJ, USA).

Western Blotting Analyses

Western blotting was performed as previously described (10). Primary antibodies were obtained for PRKR-like endoplasmic reticulum kinase (PERK; 1:1,000), inositol requiring kinase1α (IRE1α; 1:1,000), activating transcription factor 6 (ATF6; 1:1,000), caspase 4 (1:1,000), C/EBP-homologous protein (CHOP; 1:800), glucose-regulated protein 78 (GRP78; 1:1,000; Abcam, UK), p-JNK1 (1:200), JNK1 (1:200; Santa Cruz Biotechnology, Santa Cruz, CA, USA), and caspase 12 (1:1,000; Merck Millipore, Germany). The intensity of the protein bands was quantified using an ultraviolet crosslinker (Bio-Rad Laboratories, Hercules, CA, USA) and normalized to β-actin (rabbit polyclonal anti-β-actin antibodies; KeyGEN Co., Ltd., Nanjing, China).

Immunocytochemistry

Immunocytochemistry analyses were performed as previously described (13). Primary antibodies were obtained for caspase 4 (1:100) and GRP78 (1:100) (Abcam).

Tumor Implantation

The tumor implantation experiments were authorized by the Institutional Animal Care and Use Committee of Yanbian University. HepG2 cells (1×10^7 cells/0.1 ml) were injected subcutaneously into the left posterior flank of 28-day-old male BALB/c nude mice ($n = 8$) (Shanghai Laboratory Animal Co., Ltd., Shanghai, China). The greatest longitudinal diameter (length) and greatest transverse diameter (width) were measured by caliper for each tumor to estimate gross tumor volume (GTV) as $GTV = 1/2(\text{length} \times \text{width}^2)$ (14).

When the GTV reached 50–100 mm³, the mice were randomly assigned to groups that received TTF1-NPs (5, 10, or 20 μmol/kg), adriamycin (ADM; doxorubicin; 2 mg/kg), or normal saline (vehicle) every other day for 20 days (10 intravenous administrations). GTV was measured 8, 10, 12, 14, 16, 18, and 20 days after the initiation of treatment. The animals were sacrificed 20 days after the initiation of treatment to measure tumor weight and volume, from which the tumor growth ratio and tumor growth inhibition ratio were calculated as indicated below:

$$\text{tumor growth ratio } (\%) = (GTV_{T20}/GTV_{T0})/(GTV_{V20}/GTV_{V0}) \times 100$$

where GTV_{T0} and GTV_{T20} were the GTVs of the treatment group before treatment and on day 20, respectively, and GTV_{V0} and GTV_{V20} were the GTVs of the vehicle group before treatment and on day 20, respectively.

$$\text{tumor growth inhibition ratio } (\%) = (TW_{\text{vehicle}} - TW_{\text{treatment}})/TW_{\text{vehicle}} \times 100$$

where TW_{vehicle} and $TW_{\text{treatment}}$ were the tumor weights of the vehicle and tumor groups, respectively.

Statistical Analyses

All data were obtained from at least three independent tests with triplicate samples and shown as mean ± SD. SPSS software version 17.0 (IBM Corporation, Armonk, NY, USA) was used for statistical analysis (one-way ANOVA for multiple groups and independent *t*-test for two groups). The threshold for significance was a value of $p < 0.05$.

RESULTS

TTF1-NPs Inhibit Human Hepatoma Cell Growth

HepG2 cells were treated with TTF1-NPs (50, 100, or 200 μM) and assayed after 24, 48, and 72 h. After 48 h, 100 μM of TTFI-NPs significantly ($p < 0.05$) inhibited HepG2 cell growth in comparison with that of the vehicle-treated cells. Moreover, the inhibitory effects of TTFI-NPs on HepG2 cells were time and dose dependent (Fig. 1A). In Hep3B and PLC/PRF/5 cells, 48 h of exposure to 200 μM TTFI-NPs significantly ($p < 0.01$) inhibited growth in comparison with that of the corresponding vehicle-treated cells (Fig. 1B, C). TTF1-NPs at 50, 100, and 200 μM did not significantly inhibit the growth of human liver cells (Chang cell line) in comparison with that of vehicle-treated cells (Fig. 1D). The IC$_{50}$ value of TTF1-NPs against HepG2, Hep3B, and PLC/PRF/5 cells is 98.26, 114.5, and 109.9 μmol/L, respectively.

TTF1-NPs Inhibit HepG2 Tumor Growth in Nude Mice

Because TTF1-NPs showed a significant inhibitory effect on human hepatoma cells, we tested their effects on implanted HepG2 cell tumor growth in nude mice. As shown in Figure 2A, TTF1-NP-treated mice (5, 10, and 20 μmol/kg) showed GTV significantly smaller than that of the vehicle-treated mice after 16 ($p < 0.05$), 18 ($p < 0.01$), and 20 ($p < 0.01$) days of treatment. The tumors were collected and weighed after 20 days of treatment (Fig. 2B), and the tumors of the TTF1-NP-treated mice were significantly lighter than those of the vehicle-treated mice ($p < 0.01$ for 20 μmol/kg TTF1-NPs, $p < 0.05$ for 5 and 10 μmol/kg TTF1-NPs) (Fig. 2C, D). In addition, the tumor growth ratio of the TTF1-NP-treated mice was significantly ($p < 0.01$) lower than that of the vehicle-treated mice (Fig. 2E), and the tumor growth inhibition ratio of the TTF1-NP-treated mice was significantly ($p < 0.01$) higher than that of the vehicle-treated mice (Fig. 2F).

TTF1-NPs Induce Apoptosis in HepG2 Cells

Because TTF1-NPs inhibited tumor growth in vitro and in vitro, we performed experiments aimed at elucidating the mechanism underlying this effect. H&E staining of TTF1-NP-treated HepG2 cells showed altered cell morphology and pyknosis (Fig. 3A). In comparison with the number of vehicle-treated HepG2 cells, there were
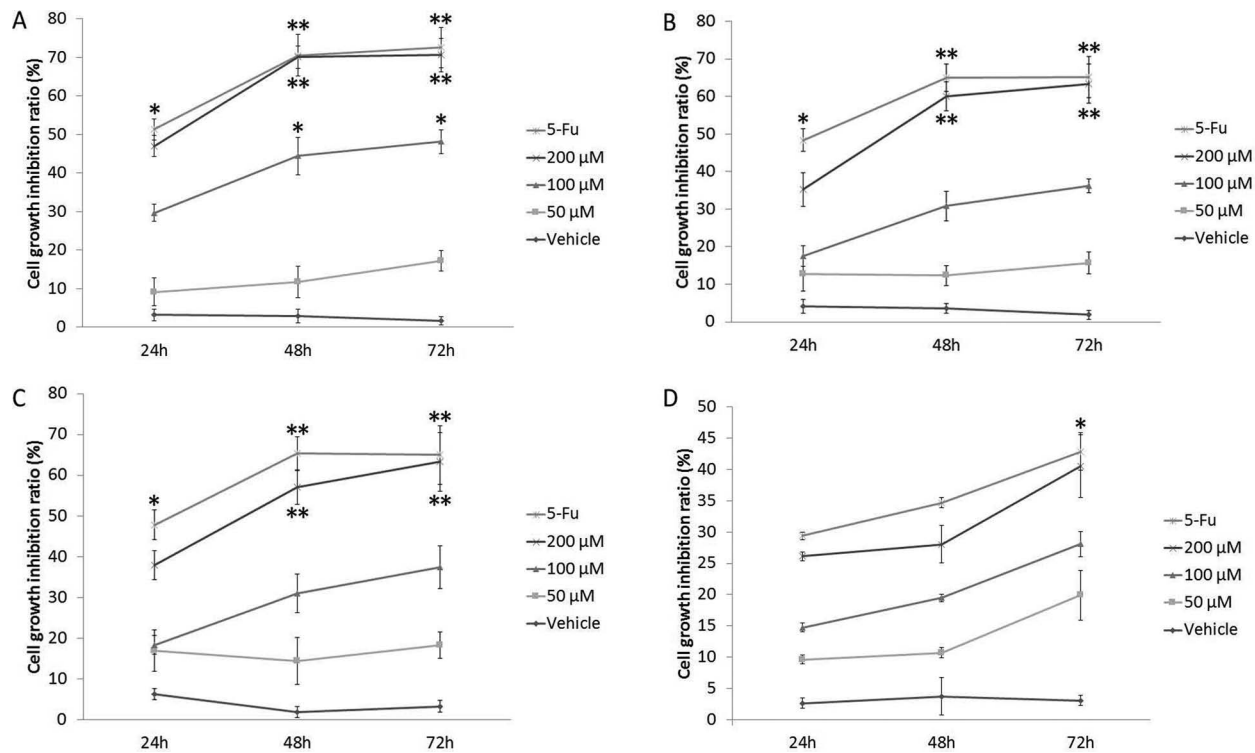
Figure 1. TTF1-NPs inhibit human hepatoma cell growth. After 24, 48, and 72 h of treatment with TTF1-NPs (50, 100, and 200 μM), 10 μM 5-fluorouracil (5-FU), or DMEM medium (vehicle), the cell growth inhibition ratios (%) for human hepatoma cells and liver cells were calculated. (A) HepG2 cells, (B) Hep3B cells, (C) PLC/PRF/5 cells, and (D) human liver cells (Chang cell line). Results are presented as mean±SD from three independent tests with triplicate samples. *$p < 0.05$ and **$p < 0.01$ for the designated treatment versus vehicle.

significantly fewer cells treated with 100 μM ($p < 0.05$) and 200 μM ($p < 0.01$) of TTF1-NPs (Fig. 3D). Hoechst staining showed clear blue fluorescence in the nuclei of cells treated with 100 or 200 μM TTF1-NPs, but almost no blue fluorescence was observed in the vehicle-treated cells (Fig. 3B), suggesting that apoptosis occurred in the TTF1-NP-treated HepG2 cells. Quantification of the number of blue fluorescence-positive (BFP) cells in the groups shown in Figure 3B demonstrated that there were fewer BFP HepG2 cells in the groups treated with TTF1-NPs (100 or 200 μM) in comparison with the vehicle-treated group (Fig. 3E).

Flow cytometry was performed to quantify the apoptosis rate in HepG2 cells (Fig. 3C), and the apoptosis rate was calculated as shown in Figure 3F. In comparison with the apoptosis rate of the vehicle-treated cells (7.63 ± 9.85%), the apoptosis rates of the cells treated with 50 μM TTF1-NPs (39.28 ± 10.81%; $p < 0.05$), 100 μM TTF1-NPs (68.11 ± 15.89%; $p < 0.01$), or 200 μM TTF1-NPs (73.43 ± 17.39%; $p < 0.01$) were significantly increased. There was no significant difference ($p > 0.05$) in the apoptosis rate of the cells treated with 200 μM TTF1-NPs and those treated with positive control drug 5-FU (92.00 ± 2.66%).

Inhibition of ERS Activation Blocks TTF1-NP-Induced Apoptosis in HepG2 Cells

To investigate the mechanism by which TTF1-NPs induced apoptosis in HepG2 cells, we analyzed expression of the ERS initial response signaling protein GRP78 and the ERS-specific proapoptotic protein caspase 4 in HepG2 cells using immunocytochemistry. GRP78-positive and caspase 4-positive cells were observed in the group treated with 200 μM TTF1-NPs (Fig. 4A, B). To quantify the expression of GRP78 and caspase 4 and investigate the expression of other ERS-related signaling molecules (PERK, IRE1α, and ATF6) and apoptosis mediators (JNK, p-JNK, and CHOP) in TTF1-NP-treated HepG2 cells, Western blotting was performed (Fig. 4C). In comparison with the vehicle-treated cells, the cells treated with 200 μM TTF1-NPs showed significantly increased expression of GRP78 ($p < 0.01$), PERK ($p < 0.05$), IRE1α ($p < 0.05$), ATF6 ($p < 0.05$), caspase 4 ($p < 0.01$), and CHOP ($p < 0.01$) (Fig. 4D), while the cells treated with 100 μM TTF1-NPs showed significantly increased expression of GRP78 ($p < 0.05$), IRE1α ($p < 0.05$), and ATF6 ($p < 0.05$) (Fig. 4D).

To confirm the involvement of ERS in TTF1-NP-induced apoptosis, we tested the effect of ERS inhibition
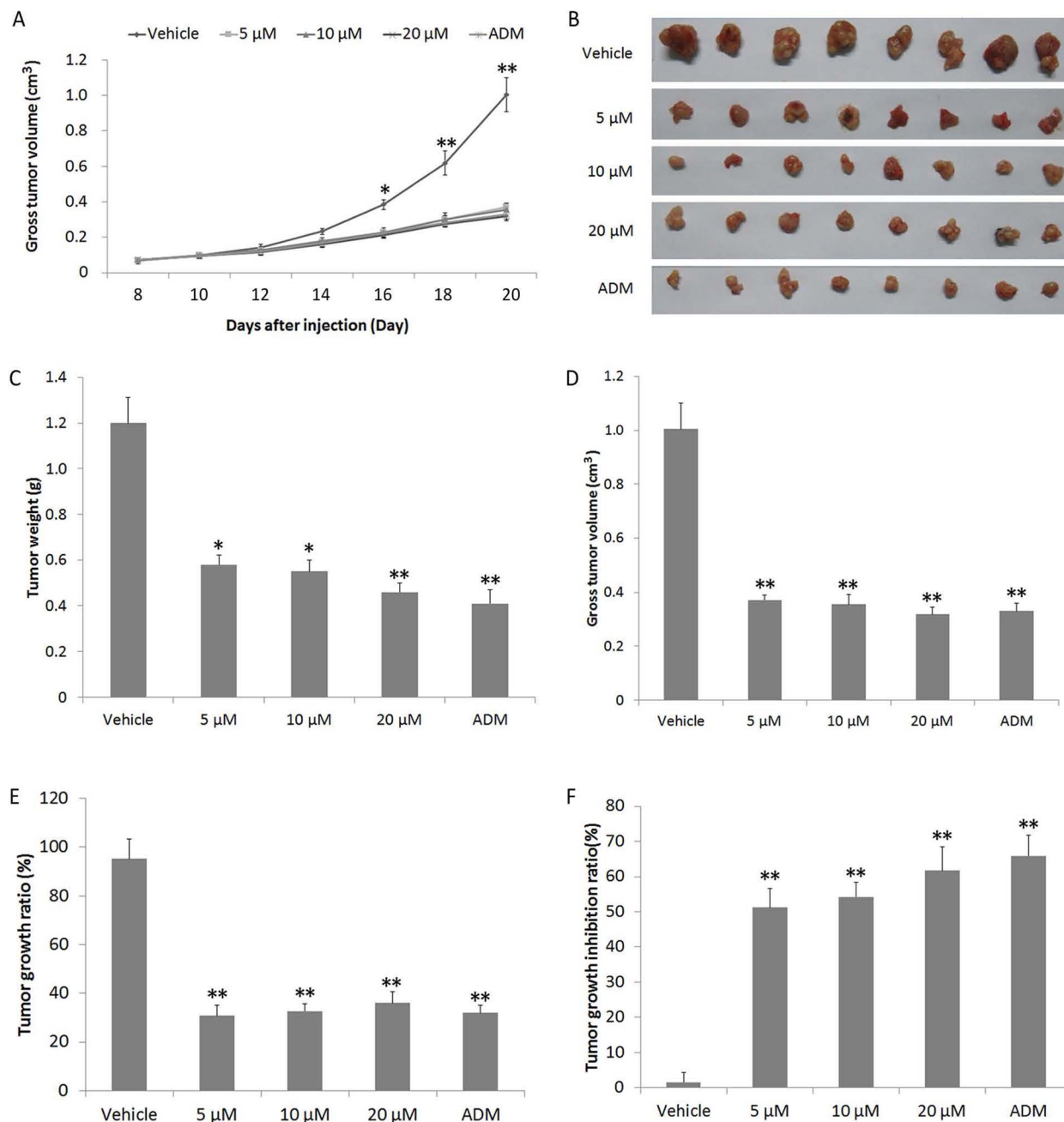
Figure 2. TTF1-NPs inhibit the growth of tumors from HepG2 cells implanted into nude mice. (A) Dynamic changes in gross tumor volume (GTV) in HepG2 cells implanted into nude mice after 8, 10, 12, 14, 16, 18, and 20 days of treatment (every other day) with TTF1-NPs (10 administrations at 5, 10, or 20 μmol/kg), adriamycin (ADM, 10 administrations at 2 mg/kg), or saline (vehicle). (B) Tumors were obtained from nude mice ($n=8$) after 20 days of treatment, and (C) tumor weight (g) and GTV (cm³) were determined. (E) Tumor growth ratio (%) was calculated based on the GTV data. (F) Tumor growth inhibition ratio (%) was calculated based on the tumor weight data. The results are shown as mean±SD from eight independent samples. *$p<0.05$ and **$p<0.01$ for the designated treatment versus vehicle.

in TTF1-NP-treated (200 μM) HepG2 cells using the ERS inhibitor 4-PBA. The apoptosis rate of the TTF1-NP-treated cells pretreated with 4-PBA was significantly decreased (Fig. 4E) in comparison with that of the TTF1-NP-treated cells that were not pretreated with 4-PBA. Moreover, protein levels of GRP 78, caspase 4, and p-JNK were significantly decreased in cells treated with 200 μM TTF1-NPs and 4-PBA in comparison with those treated with 200 μM TTF1-NPs alone (Fig. 4F, G).
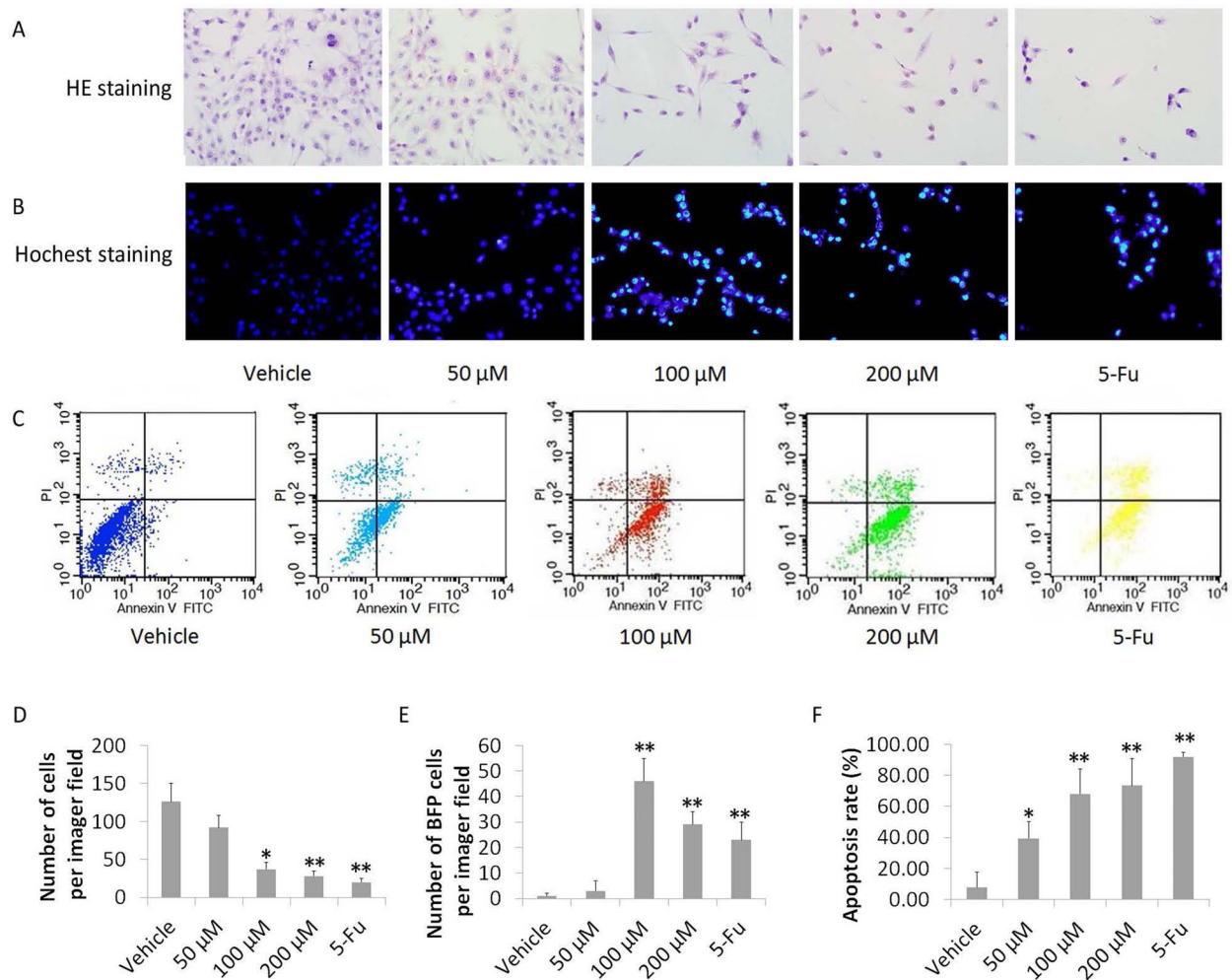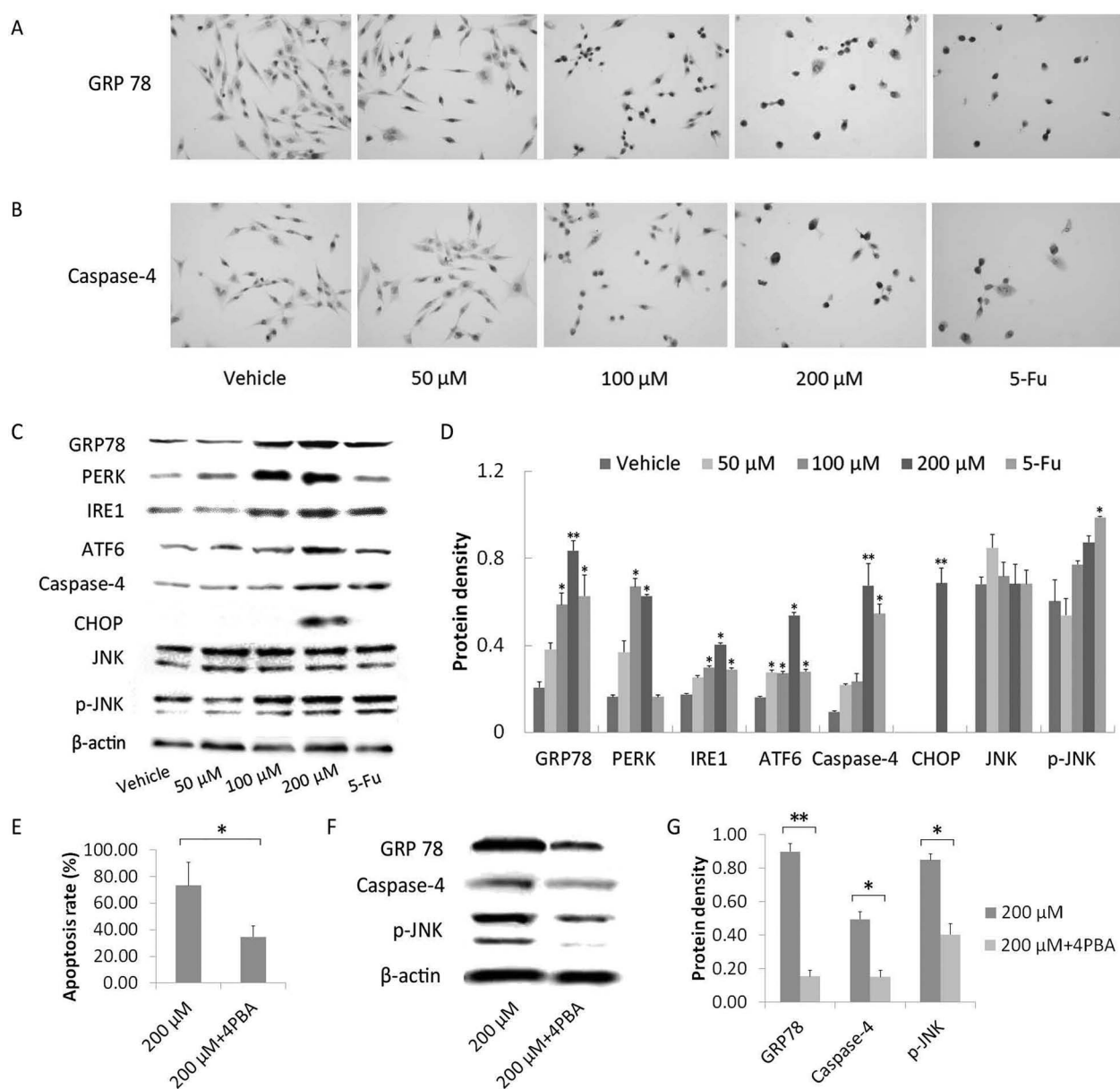
Figure 3. TTF1-NPs induce apoptosis in HepG2 cells. HepG2 cells treated with TTF1-NPs (50, 100, or 200 μM), 10 μM 5-fluorouracil (5-FU), or DMEM (vehicle) for 48 h were subjected to (A) hematoxylin and eosin staining (400× magnification), (B) Hoechst staining (400× magnification), and (C) flow cytometry. (D) Quantification of cell numbers from the fields shown in (A) was performed using three independent tests with triplicate samples. (E) Quantification of blue fluorescence-positive (BFP) cell numbers from the fields shown in (B) was performed using three independent tests with triplicate samples. (F) Quantification of cell apoptosis rate (%) was performed based on the results shown in (C) from three independent tests with triplicate samples. The graph shows the corresponding quantified data as mean ± SD. *$p < 0.05$ and **$p < 0.01$ for the designated treatment versus vehicle.

DISCUSSION

In the past decade, the endoplasmic reticulum stress (ERS) response has been increasingly exploited as a mechanism for anticancer drugs because studies show that this response is an important facilitator of solid tumor growth under stressful conditions commonly encountered by such tumors, including glucose deprivation and hypoxia (15,16). In this study, we tested the hypothesis that TTF1-NPs produced from TTF1, the primary anticancer component of *S. sorbifolia*, are an effective therapy against HCC in vivo and in vitro that act by inducing apoptosis. Moreover, we explored the involvement of the ER stress response as a mediator of TTF1-NP-induced apoptosis because we have previously shown that TTF1

induced apoptosis via a mitochondrial pathway, but this pathway did not seem to be completely responsible for the proapoptotic effects of TTF1 (10).

TTF1-NPs produced dose- and time-dependent inhibitory effects on HepG2 cell growth, and 100 μM of TTF1-NPs significantly inhibited cell growth after 48 h. TTF1-NPs seemed to be less potent in Hep3B and PLC/PRF/5 cells, but 200 μM TTF1-NPs significantly inhibited growth in both of these cell lines. In contrast, TTF1-NPs did not inhibit the growth of human liver cells, demonstrating its specificity for tumor cells over normal cells. These results confirmed our expectation that TTF1-NPs would inhibit human hepatoma cell growth, which was based on our previous studies (9).

Figure 4. Inhibition of ERS blocked TTF1-NP-induced HepG2 cell apoptosis. HepG2 cells treated with TTF1-NPs (50, 100, or 200 μM), 10 μM 5-fluorouracil (5-FU), or DMEM (vehicle) for 48 h were subjected to immunocytochemical staining for (A) GRP78 and (B) caspase 4 (400× magnification), as well as (C) Western blot analysis. (D) ERS-related proteins were quantified from three independent tests with triplicate samples. (E) Quantification of apoptosis rate (%) in TTF1-NP-treated (200 μM) cells without 4-PBA treatment and in TTF1-NP-treated (200 μM) cells pretreated with 4-PBA. (F) Expression of GRP78, caspase 4, and p-JNK in TTF1-NP-treated (200 μM) cells without 4-PBA treatment and in TTF1-NP-treated (200 μM) cells pretreated with 4-PBA. (G) The results shown for GRP78, caspase 4, and p-JNK in (F) were quantified from three independent tests with triplicate samples. The graph shows the corresponding quantified data as mean ± SD. *$p < 0.05$ and **$p < 0.01$ for the designated treatment versus vehicle (D) or for the designated treatment versus 200 μM TTF1-NPs (E, G).

After confirming that TTF1-NPs showed a significant inhibitory effect on human hepatoma cells, we tested their effects on implanted HepG2 cell tumor growth in nude mice (17). At doses of 5, 10, and 20 μmol/kg, TTF1-NPs significantly reduced GTV in comparison with vehicle after 16, 18, and 20 days of treatment. Moreover, the tumors of the TTF1-NP-treated mice were significantly lighter than those of the vehicle-treated mice at all tested doses after 20 days of treatment. Finally, the TTF1-NP-treated mice showed a significantly reduced tumor growth ratio and a significantly increased tumor growth inhibition ratio, in comparison with those of the

vehicle-treated mice. These in vivo results demonstrate that TTF1-NPs produce antitumor effects in animals, corroborating our in vitro results. Moreover, these results confirm that nanoparticle formulations can be used to improve the pharmacokinetic and pharmacodynamic characteristics of anticancer compounds (18), including compounds from natural products that may not be ideal for in vivo therapeutic use in their raw form (19,20).

To demonstrate that our TTF1-NP formulation produced antitumor effects by inducing apoptosis, as we previously demonstrated for TTF1 (10), we performed cell morphology and flow cytometry studies using HepG2 cells. Confirming our previous results, H&E and Hoechst staining showed that TTF1-NPs at concentrations of 100 or 200 μM altered cell morphology and induced pyknosis. Moreover, flow cytometry showed that TTF1-NPs induced apoptosis dose dependently at concentrations from 50 to 200 μM, and no significant difference was found between the effect of 200 μM TTF1-NPs and that of the positive control drug 5-FU.

We have previously demonstrated that TTF1 induced apoptosis via a mitochondrial pathway; however, several proapoptotic pathways exist in mammalian cells that may be exploited in tumor cells to induce death (21–23). Therefore, we used Western blotting and immunohistochemistry to further investigate the mechanism by which TTF1-NPs induce apoptosis by measuring levels of specific apoptosis-related proteins. The ERS response, the endogenous mitochondrial pathway, and the exogenous death receptor pathway are the three major independent apoptotic pathways in eukaryotic cells (24–26). The endoplasmic reticulum is kept in dynamic equilibrium under normal physiological conditions, but pathological and physiological stimuli can induce imbalance in endoplasmic reticulum homeostasis and thus induce the ERS response. The ERS response is primarily mediated by the molecular chaperone GRP78 and three transmembrane signaling molecules: PERK, IRE1α, and ATF6 (27). When misfolded and unfolded proteins accumulate in the ER and threaten to disrupt proper protein folding, the insufficient supply of GRP78 leads to activation of the unfolded protein response (UPR) (28,29) and ER-associated degradation (ERAD) of misfolded proteins through the ubiquitin proteasome system, thus alleviating ER dysfunction (30,31). However, under conditions of prolonged ER stress, the function of the UPR shifts from prosurvival to proapoptotic, and this proapoptotic potential can be exploited as a therapeutic mechanism for anticancer drugs (15).

The primary apoptotic pathway utilized by the UPR is mediated by the CHOP transcription factor, which is uniquely responsive to ERS (32). Under conditions of ERS, GRP78 dissociates from PERK, IRE1, and ATF6, allowing PERK and IRE1 to homodimerize and become activated via self-phosphorylation. Activated PERK phosphorylates eIF2α, leading to inhibition of translation, cell cycle arrest,

and activation of the downstream signaling molecule ATF4 as part of the PERK-eIF2α-ATF4 complex, which induces CHOP expression (33). Moreover, activated IRE1α activates apoptosis signal-regulating kinase 1 (ASK1) by recruiting TNF-α receptor-associated factor 2 (TRAF2), thus inducing CHOP expression. Upon dissociation from GRP78, ATF6 is activated by proteolytic cleavage inside the Golgi apparatus, after which the activated ATF6 fragment translocates to the nucleus and forms a complex with transcription factor X-box-binding protein 1 (XBP1), which directly activates CHOP expression (33).

The second apoptotic pathway utilized by the UPR is mediated by c-Jun N-terminal kinases (JNKs). Upon dissociation from GRP78, activated IRE-1 forms the IRE-1-TRAF2-ASK1 complex, which phosphorylates JNK1, promoting apoptosis (32). The third apoptotic pathway utilized by the UPR is a caspase-mediated pathway involving caspase 12. Activated IRE1 recruits T33RAF2 located at the ER membrane to cleave the caspase 12 precursor into an activated caspase 12 fragment, which is an ERS-specific proapoptotic factor. Upon activation, caspase 12 activates downstream caspase family members to induce an apoptotic cascade. Animal studies have shown that the functions of caspase 4 in humans are equivalent to those of caspase 12 in rodents. Studies on the diverse apoptotic mechanisms utilized by the UPR demonstrate that GRP78, CHOP, JNK1, and caspase 12 (caspase 4 in humans) are key mediators of ERS-related apoptosis (32,34).

Confirming our hypothesis that TTF1-NPs induce apoptosis via ERS, treatment with 200 μM TTF1-NPs significantly increased the proportion of GRP78-positive and caspase 4-positive cells. Moreover, treatment with 200 μM TTF1-NPs significantly upregulated GRP78, PERK, IRE1α, ATF6, caspase-4, and CHOP, while 100 μM TTF1-NPs upregulated only GRP78, IRE1α, and ATF6, demonstrating dose-related effects on proapoptotic signaling. To further strengthen our results, we examined the effect of ERS inhibitor 4-PBA, a low molecular weight fatty acid that acts as a chemical chaperone, preventing or reversing aggregation and mislocalization of misfolded proteins in the ER. In our study, 4-PBA significantly decreased the apoptosis rate in TTF1-NP-treated cells and inhibited regulation of apoptosis-related proteins by TTF1-NPs. The expression levels of key proteins includes GRP78, caspase 4, p-JNK, and CHOP in HepG2 xenograft tumor tissues were significantly increased in TTF1-NP-treated groups compared to the vehicle group. These results suggest that ERS plays a central role in TTF1-NP-induced apoptosis in vivo and in vitro demonstrating that TTF1 may induce apoptosis in tumor cells via multiple mechanisms.

Our study has some limitations as a result of limited time and resources. We have only tested TTF1-NPs in a

limited number of hepatoma cell types, including the HepG2, Hep3B, and PLC/PRF/5 cell lines. However, HCC shows significant variation in characteristics among patients, and thus our results may not be generalizable to all types of HCC in all patients, despite our promising results. In a related limitation, we implanted only HepG2 cells into mice, and it should be noted that these cells were also the most susceptible of the tested cell lines to TTF1-NPs. In addition, we tested the effects of TTF1-NPs on implanted tumors in mice only, and the use of other model organisms, such as rats or rabbits, would strengthen our conclusions. Finally, we tested the off-target effects of TTF1-NPs in only one cell type, limiting the strength of our conclusions regarding toxicity in normal cells.

Future studies should address the limitations of our study, with the goal of providing sufficient evidence for the efficacy of TTF1-NPs against HCC to merit clinical trials. Toward this end, studies should be conducted on other hepatoma cell types using a larger range of TTF1-NP doses and longer period of treatment and observation. In addition, in vivo studies of longer duration in other animal models will allow for investigation of the long-term efficacy of TTF1-NPs and associated toxicity. Evaluation of toxicity is particularly important because toxicity may underlie the failure of current treatments such as sorafenib to improve quality of life, and thus lower toxicity would represent a significant advantage for TTF1-NPs (7). Toxicology studies should be performed on other normal cell types and in vivo to determine off-target effects of TTF1-NPs and maximum tolerated doses. Future studies with knockout mice and inhibitors of specific signaling pathways would allow for finer dissection of the mechanism underlying the proapoptotic effects of TTF1-NPs, which seem to be mediated by multiple pathways. Finally, in silico modeling to explore the pharmacodynamics of TTF1 will facilitate the development of more effective anticancer drugs.

Taken together, our results demonstrate that TTF1-NPs generated from TTF1, the primary bioactive constituent of *Sorbaria sorbifolia*, are a promising new therapeutic vector for HCC that merits extensive further study in vivo and in vitro.

REFERENCES

1. Venook, A. P.; Papandreou, C.; Furuse, J.; de Guevara, L. L. The incidence and epidemiology of hepatocellular carcinoma: A global and regional perspective. Oncologist 4:5–13; 2010.

2. Kremsdorf, D.; Soussan, P.; Paterlini-Brechot, P.; Brechot C. Hepatitis B virus-related hepatocellular carcinoma: Paradigms for viral-related human carcinogenesis. Oncogene 25:3823–3833; 2006.

3. Sanyal, J.; Yoon, S. K.; Lencioni R. The etiology of hepatocellular carcinoma and consequences for treatment. Oncologist 4:14–22; 2010.

4. El-Serag, H.; Rudolph, K. L. Hepatocellular carcinoma: Epidemiology and molecular carcinogenesis. Gastroenterology 132:2557–2576; 2007.

5. Chen, X.; Liu, H. P.; Li, M.; Qiao, L. Advances in nonsurgical management of primary liver cancer. World J. Gastroenterol. 20:16630–16638; 2014.

6. Zhu, A. X. Systemic therapy of advanced hepatocellular carcinoma: How hopeful should we be? Oncologist 11:790–800; 2006.

7. Keating, G. M.; Santoro, A. Sorafenib: A review of its use in advanced hepatocellular carcinoma. Drugs 69:223–240; 2009.

8. Ling, C.; Chiu, J.; Oh, B.; Cho, W. C. S. Natural products for liver diseases: Basic, clinical, and translational research. Evid. Based Complement. Alternat. Med. 2012:794343; 2012.

9. Liu, C.; Li, X-W.; Cui, L-M.; Li, L-C.; Chen, L-Y.; Zhang, X-W. Inhibition of tumor angiogenesis by TTF1 from extract of herbal medicine. World J. Gastroenterol. 17:875–882; 2011.

10. Li, Y.; Lei, B.; Cui, F-D.; Li, L-C.; Zhang, X-W. TTF1-induced apoptosis of HepG-2 cells through a mitochondrial pathway. Oncol. Rep. 26:651–657; 2011.

11. Li, Y.; Cui, F. D.; Zhang X. W. Preparation technology of Sorbaria sorbifolia solid lipid nanoparticles. Lishizhen Med. Materia. Medica Res. 23:2459–2450; 2012.

12. Jia, L. J.; Zhang, D. R.; Li, Z. Y.; Feng, F. F.; Wang, Y. C.; Dai, W. T.; Duan, C. X.; Zhang, Q. Preparation and characterization of silybin-loaded nanostructured lipid carriers. Drug Deliv. 17:11–18; 2010.

13. van Malenstein, H.; Verslype, C.; Windmolders, P.; van Eijsden, R.; Nevens, F.; van Pelt, J. Characterization of a cell culture model for clinically aggressive hepatocellular carcinoma induced by chronic. Cancer Lett. 315:178–188; 2012.

14. Rao, J., Zhou, Z. H.; Yang, J., Shi, Y., Xu, S. L.; Wang, B.; Ping, Y. F.; Chen, L.; Cui, Y. H.; Zhang, X.; Wu, F.; Bian, X. W. Semaphorin-3F suppresses the stemness of colorectal cancer cells by inactivating Rac1. Cancer Lett. 358:76–84; 2015.

15. Healy, S. J.; Gorman, A. M.; Mousavi-Shafaei, P.; Gupta, S.; Samali, A. Targeting the endoplasmic reticulum-stress response as an anticancer strategy. Eur. J. Pharmacol. 625:234–246, 2009.

16. Boelens, J.; Lust, S.; Offner, F.; Bracke, M. E.; Vanhoecke, B. W. The endoplasmic reticulum: A target for new anticancer drugs. In Vivo 21:215–226; 2007.

17. Zhang, D. W.; Li, H. Y.; Lau, W. Y.; Cao, L. Q.; Li, Y.; Jiang, X. F.; Yang, X. W.; Xue, P. Gli2 silencing enhances TRAIL-induced apoptosis and reduces tumor growth in human hepatoma cells in vivo. Cancer Biol. Ther. 15:1667–1676; 2014.

18. Yamamoto, Y.; Hyodo, I.; Koga, Y.; Tsumura, R.; Sato, R.; Obonai. T.; Fuchigami, H.; Furuya, F.; Yasunaga, M.; Harada, M.; Kato, Y.; Harada, M.; Matsumura, Y. Enhanced antitumor effect of anti-tissue factor (TF) antibody-conjugated epirubicin-incorporating micelles in xenograft models. Cancer Sci. 106(5):627–634; 2015.

19. Dikmena, G.; Güney, G.; Genç, L. Characterization of solid lipid nanoparticles containing caffeic acid and determination

of its effects on MCF-7 cells. Recent Pat. Anticancer Drug Discov. 10(2):224–232; 2015.

20. Huang, W.; Wang, X.; Shi, C.; Guo, D.; Xu, G.; Wang, L.; Bodman, A.; Luo J. Fine-tuning vitamin E-containing telodendrimers for efficient delivery of gambogic acid in colon cancer treatment. Mol. Pharm. 12(4):1216–1229; 2015.

21. Naik, S.; MacFarlane, M.; Sarin, A. Notch4 signaling confers susceptibility to TRAIL induced apoptosis in breast cancer cells. J. Cell Biochem. 116(7):1371–1380; 2015.

22. Tian, R. Li, Y.; Gao, M. Shikonin causes cell cycle arrest and induces apoptosis by regulating the EGFR/NF- B signaling pathway in human epidermoid carcinoma A431 cells. Biosci. Rep. 35(2):e00189; 2015.

23. Montero, J.; Sarosiek, K. A.; DeAngelo, J. D.; Maertens, O.; Ryan, J.; Ercan, D.; Piao, H.; Horowitz, N. S.; Berkowitz, R. S.; Matulonis, U.; Jänne, P. A.; Amrein, P. C.; Cichowski, K.; Drapkin, R.; Letai, A. Drug-induced death signaling strategy rapidly predicts cancer response to chemotherapy. Cell 160:977–989; 2015.

24. Fulda, S. Safety and tolerability of TRAIL receptor agonists in cancer treatment. Eur. J. Clin. Pharmacol. 71(5):525–527; 2015.

25. Notte, A.; Rebucci, M.; Fransolet, M.; Roegiers, E.; Genin, M.; Tellier, C.; Watillon, K.; Fattaccioli, A.; Arnould, T.; Michiels, C. Taxol-induced unfolded protein response activation in breast cancer cells exposed to hypoxia: ATF4 activation regulates autophagy and inhibits apoptosis. Int. J. Biochem. Cell Biol. 62:1–14; 2015.

26. Lei, K.; Tan, S.; Du, W.; Xu, Y.; Lin, S.; Zheng, Y.; Zou, F.; Xu, Y.; Liu, J. 3B, a novel of photosensitizer, exhibited anti-tumor effects via mitochondrial apoptosis pathway in MCF-7 human breast carcinoma cells. Tumour Biol. 36(7):5597–5606; 2015.

27. Ulianich, L.; Insabato, L. Endoplasmic reticulum stress in endometrial cancer. Front. Med. (Lausanne) 1:55; 2014.

28. Mesitov, M.; Moskovtsev, A. A.; Kubatiev, A. A. Molecular logic of the endoplasmic reticulum stress signal pathways: The system of unfolded protein response. Patol. Fiziol. Eksp. Ter. 4:97–108; 2013.

29. Manié, S.; Lebeau, J.; Chevet, E. Cellular mechanisms of endoplasmic reticulum stress signaling in health and disease. 3. Orchestrating the unfolded protein response in oncogenesis: An update. Am. J. Physiol. 307:C901–907; 2014.

30. Zattas, D.; Hochstrasser, M. Ubiquitin-dependent protein degradation at the yeast endoplasmic reticulum and nuclear envelope. Crit. Rev. Biochem. Mol. Biol. 50(1):1–17; 2014.

31. Liu, Y.; Ye, Y. Proteostasis regulation at the endoplasmic reticulum: A new perturbation site for targeted cancer therapy. Cell Res. 21:867–883; 2011.

32. Afrin, R.; Arumugam, S.; Soetikno, V.; Thandavarayan, R. A.; Pitchaimani, V.; Karuppagounder, V.; Sreedhar, R.; Harima, M.; Suzuki, H.; Miyashita, S.; Nomoto, M.; Suzuki, K.; Watanabe, K. Curcumin ameliorates streptozotocin induced liver damage through modulation of endoplasmic reticulum stress mediated apoptosis in diabetic rats. Free Radic. Res. 49:279–289; 2015.

33. Jiang, X.; Kanda, T.; Nakamoto, S.; Haga, Y.; Sasaki, R.; Nakamura, M.; Wu, S.; Mikata, R.; Yokosuka, O. Knockdown of glucose-regulated protein 78 enhances poly (ADP-ribose) polymerase cleavage in human pancreatic cancer cells exposed to endoplasmic reticulum stress. Oncol. Rep. 32:2343–2348; 2014.

34. Wang, M.; Meng, X. B.; Yu, Y. L.; Sun, G. B.; Xu, X. D.; Zhang, X. P.; Dong, X.; Ye, J. X.; Xu, H. B.; Sun, Y. F.; Sun, X. B. Elatoside C protects against hypoxia/reoxygenation-induced apoptosis in H9c2 cardiomyocytes through the reduction of endoplasmic reticulum stress partially depending on STAT3 activation. Apoptosis 19:1727–1735; 2014.